Azimuthal asymmetry of the extracted electron in field ionization of a hydrogen atom with orbital angular momentum

X. Artru[1,*] and E. Redouane-Salah[2,3,4,†]

[1]*Université de Lyon, CNRS/IN2P3 and Université Lyon 1, Institut de Physique Nucléaire de Lyon, 69622 Villeurbanne, France*

[2]*Faculté des Sciences, Département de Physique, Université de M'sila, M'sila, Algeria*

[3]*Lawrence Berkeley National Laboratory, University of California, Berkeley, California 94720, USA*

[4]*Laboratoire de physique mathématique et physique subatomique, Université de Constantine 1, Constantine, Algeria*

(Received 14 December 2015; published 3 February 2016)

The tunneling ionization of an excited hydrogen atom by a static electric field $\mathbf{E}$ is investigated for the case where the initial electron has an orbital angular momentum $\mathbf{L}$ nonparallel to $\mathbf{E}$. The outgoing electron has a nonzero mean transverse velocity $\langle \mathbf{v}_T \rangle$ in the direction of $\mathbf{E} \times \langle \mathbf{L} \rangle$. During this process the linear Stark effect makes $\langle \mathbf{L} \rangle$ and $\langle \mathbf{v}_T \rangle$ oscillate or rotate about $\mathbf{E}$. Measures of the asymmetry are calculated at leading order in $\mathbf{E}$ for an initial state $2P$ state. The generalization to *coherent elliptic* Rydberg states is outlined. A subset of these states whose classical Kepler ellipses rotate rigidly about $\mathbf{E}$ is particularly interesting for the observation of the asymmetry. The preparation of states with $\mathbf{L}$ nonparallel to $\mathbf{E}$ and the conditions to get a sizable $\mathbf{v}_T$ asymmetry are discussed.

DOI: 10.1103/PhysRevA.93.023403

I. INTRODUCTION

An atom placed in a strong static electric field $\mathbf{E}$ may be ionized by tunneling if the initial electron energy is below the saddle point of the atomic and external potentials. The calculation, to lowest order (LO) in $\mathbf{E}$, of the ionization rate γ for a hydrogen atom in the ground state is given in textbooks [1]. A large amount of work has been devoted to the generalization to $n \geqslant 2$ states, with the inclusion of higher orders in $\mathbf{E}$ (see [2,3] and references therein for analytical calculations and [4–6] and references therein for numerical calculations). The distribution in transverse velocity $\mathbf{v}_T$ of the outgoing electron is also of theoretical and experimental interest. It provides a kind of photographic image of the electron wave function inside the atom [7–9]. The fringes of this distribution have been observed [10] using fields of the order of a few hundred volts per centimeter for atomic levels $n \sim 20$, just below or above the saddle point. A quadrupolar anisotropy in $\mathbf{v}_T$ has also been observed when the atom is excited with a linearly polarized light [11].

In the case where the initial electron state has an orbital angular momentum $\mathbf{L}$ at an angle to $\mathbf{E}$, a *dipolar* asymmetry is predicted [12], with $\langle \mathbf{v}_T \rangle$ being in the direction of $\langle \mathbf{L} \rangle \times \mathbf{F}$, where $\mathbf{F} = -e_0\mathbf{E}$ is the external force.[1] This effect, pictured in Fig. 1, will be referred to as the $[\mathbf{v},\mathbf{L},\mathbf{F}]$ asymmetry. An analogous effect presumably exists in high-energy hadron physics, with the proton-electron system being replaced by a quark-antiquark pair in a $^3P_0$ state and the electric field being replaced by a chromoelectric field [12,13]. In the case of the hydrogen atom, the $[\mathbf{v},\mathbf{L},\mathbf{F}]$ asymmetry is an interference between the decays of several *Stark states*. It is therefore sensitive to the relative phases of decay *amplitudes*, whereas the decay widths give only the amplitudes squared.

Purpose and layout of the paper. A preliminary study [14,15] predicted the $[\mathbf{v},\mathbf{L},\mathbf{F}]$ asymmetry for the $2P$ state of hydrogen, with an alternating time dependence because the *linear* Stark splitting makes $\langle \mathbf{L} \rangle$ oscillate. However, the required field to ionize the $2P$ state fast enough is not attainable in the laboratory. We therefore extend our study to Rydberg states, more particularly to the quasiclassical *coherent elliptic states* (CESs) [16]. We will first consider *circular* L_y (CLy) eigenstates, with $\mathbf{F}$ pointing in the $+\hat{\mathbf{z}}$ direction (we could have chosen L_x eigenstates as well). This is *a priori* the most simple choice. However, we will also consider another type of CES, which we call *rotating oblique elliptic* (ROE) states. They have *oblique* $\langle \mathbf{L} \rangle$, and their classical ellipses rotate undeformed about $\mathbf{E}$. They have some advantages for a $[\mathbf{v},\mathbf{L},\mathbf{F}]$ experiment. Estimations of the asymmetry will be made with analytical calculations at the LO approximation.

This paper is organized as follows: in Sec. II we briefly review the Stark states and CESs. Section III presents the CLy and ROE states, their evolutions in the field $\mathbf{E}$, and their decompositions in the Stark basis. Section IV deals with the preparation of the CLy and ROE states for a $[\mathbf{v},\mathbf{L},\mathbf{F}]$ experiment. In Sec. V we review the calculation of the width γ of a single Stark state at LO and using the *Gamow-Siegert* (GS) representation of Stark resonances. In addition we obtain the asymptotic phases of the GS wave functions. These phases are needed to evaluate the $[\mathbf{v},\mathbf{L},\mathbf{F}]$ asymmetry. Tunneling ionization of states with $\langle \mathbf{L}_T \rangle \neq 0$ and the resulting $[\mathbf{v},\mathbf{L},\mathbf{F}]$ asymmetry are treated in Sec. VI. Numerical results for the $n = 2$ CLy state are presented. Conditions of observability are discussed. The case of high-n CLy and ROE states is investigated. Conclusions and suggestions are made in Sec. VII.

II. REVIEW OF STARK AND COHERENT ELLIPTIC STATES

In this section we review the relevant properties of the states involved in the $[\mathbf{v},\mathbf{L},\mathbf{F}]$ asymmetry and write down their wave functions with precisely defined phases. The latter point is important since the asymmetry is an interference effect between several states. The Hamiltonian of a hydrogen atom in the static electric field $\mathbf{E} \equiv -\mathbf{F} = -F\,\hat{\mathbf{z}}$ is $\mathcal{H} = \mathcal{H}_0 - Fz$, with

*x.artru@ipnl.in2p3.fr

†eredouane@univ-msila.dz

[1] e_0 is the elementary charge, while $e \equiv \exp(1)$.

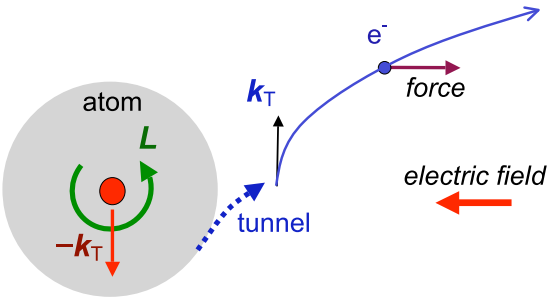

FIG. 1. Semiclassical motion of the electron extracted from the hydrogen atom by a strong field **E** when the electron is initially in a $L_y = +1$ state.

$\mathcal{H}_0 = \mathbf{p}^2/2 - 1/r$ in atomic units.[2] Relativistic and radiative corrections like spin-orbit and Lamb shifts are neglected. We make the analytic calculations at lowest order (LO) in F. In parabolic coordinates[3] $\xi = r - z$, $\eta = r + z$, $\varphi = \arg(x + iy)$, the eigenstates of $\mathcal{H}$ and L_z and the Schrödinger equation have the separable form [1,17]

$$\Psi(\mathbf{r}) = \mathcal{N}\,\xi^{-1/2}\,\chi(\xi)\,\eta^{-1/2}\,\Theta(\eta)\,e^{im\varphi}\,, \tag{1}$$

$$\frac{\partial^2\Theta}{\partial\eta^2} + \left[\frac{\mathcal{E}}{2} + \frac{Z_\eta}{\eta} - \frac{m^2-1}{4\eta^2} + \frac{F\eta}{4}\right]\Theta(\eta) = 0, \tag{2}$$

together with a similar equation for $\chi(\xi)$ with $F \to -F$ and $Z_\xi = 1 - Z_\eta$. $\mathcal{E} = -1/(2\nu^2)$ is the energy, and $\mathcal{N} = 2|\mathcal{E}|\sqrt{\pi}$ is a normalization coefficient. We introduce the new variables[4] $\sqrt{\xi/\nu} = \check{r}$, $\sqrt{\eta/\nu} = \check{R}$, $\check{x} + i\,\check{y} = \check{r}\,e^{i\varphi_1}$, and $\check{X} + i\check{Y} = \check{R}\,e^{i\varphi_2}$ with the constraint $\varphi_1 + \varphi_2 = \varphi$. The functions

$$\check{\chi}(\check{x},\check{y}) = \xi^{-1/2}\chi(\xi)\,e^{im\varphi_1}, \quad \check{\Theta}(\check{X},\check{Y}) = \eta^{-1/2}\Theta(\eta)\,e^{im\varphi_2} \tag{3}$$

are stationary functions of two two-dimensional (2D) *anharmonic* oscillators [19]:

$$[2\lambda + \Delta - \check{r}^2 - \nu^3 F\,\check{r}^4]\check{\chi}(\check{x},\check{y}) = 0\,, \tag{4a}$$

$$[2\mu + \Delta - \check{R}^2 + \nu^3 F\,\check{R}^4]\check{\Theta}(\check{X},\check{Y}) = 0\,. \tag{4b}$$

They have the same orbital angular momentum $L_z = m$; their "energies"[5] $\lambda = 2\nu\,Z_\xi$ and $\mu = 2\nu\,Z_\eta$ are linked by $\lambda + \mu = 2\nu$. The angles φ_1 and φ_2 were defined above up to a transformation $\varphi_1 \to \varphi_1 + \delta\varphi$, $\varphi_2 \to \varphi_2 - \delta\varphi$; from now on we fix $\varphi_1 = \varphi$, $\varphi_2 = 0$. Then Eq. (1) can be rewritten as

$$\Psi(\mathbf{r}) = \mathcal{N}\,\check{\chi}(\check{x},\check{y})\,\check{\Theta}(\check{R},0)\,. \tag{5}$$

We will also use the mixed representation

$$\Psi(\mathbf{r}) = \mathcal{N}\,\check{\chi}(\check{x},\check{y})\,\Theta(\eta)/\sqrt{\eta}\,. \tag{6}$$

Stark states $|n_\xi,n_\eta,m\rangle$ are eigenstates of H at LO, neglecting ionization. n_ξ and n_η are the numbers of nodes of $\chi(\xi)$ and

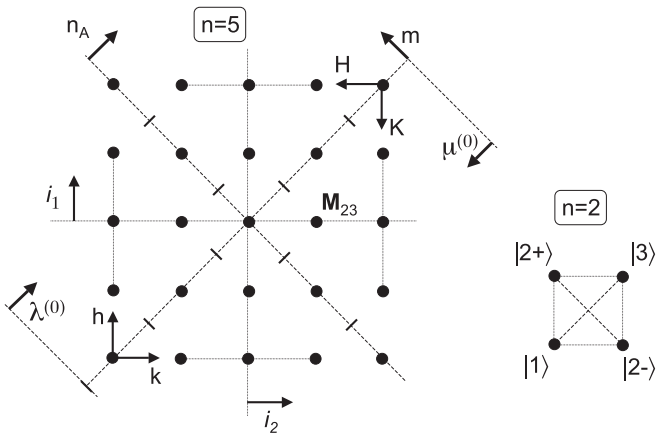

FIG. 2. The $\{h,k\}$ lattices of Stark states for $n = 5$ and 2. The top right (bottom left) corner represents the long-lived blue (short-lived red) state. The $n = 2$ states are those of Eq. (9).

$\Theta(\eta)$. The Stark wave functions are obtained by putting for $\check{\chi}$ and $\check{\Theta}$ in (5) the 2D *harmonic* oscillator wave functions Φ [20]:

$$\check{\chi} \to \Phi_{h,k}(\check{x},\check{y}) = (\pi\,h!\,k!)^{-1/2}\,(a_+^\dagger)^h\,(a_-^\dagger)^k\,e^{-(\check{x}^2+\check{y}^2)/2}, \tag{7}$$

where the operator $a_\pm^\dagger = [x - \partial_x \pm i(y - \partial_y)]/2$ creates one quantum of clockwise $(-)$ or counterclockwise $(+)$ excitation. h,k are the numbers of these quanta. Similarly, $\check{\Theta} \to \Phi_{H,K}(\check{X},\check{Y})$. In the $F \to 0$ limit,

$$\begin{aligned}
&\mathcal{E} \to -1/(2n^2)\,,\\
&\nu \to n = n_\eta + n_\xi + |m| + 1\,,\\
&\lambda \to \lambda^{(0)} = n + n_A = 2n_\xi + |m| + 1 = h + k + 1\,,\\
&\mu \to \mu^{(0)} = n - n_A = 2n_\eta + |m| + 1 = H + K + 1\,.
\end{aligned} \tag{8}$$

$n_A \equiv n_\xi - n_\eta$ is the *electric number*. $\mathcal{N}$ in Eqs. (1), (5), and (6) is chosen such that $\langle\Psi|\Psi\rangle = 1$ for Stark states. For $n = 2$ the Stark wave functions $\Psi_{n_\xi,n_\eta,m}$ are

$$\begin{aligned}
\Psi_{0,1,0} &= 8^{-1}\pi^{-1/2}\,e^{-(\xi+\eta)/4}\,(\eta - 2) \equiv \Psi_1,\\
\Psi_{0,0,\pm1} &= 8^{-1}\pi^{-1/2}\,e^{-(\xi+\eta)/4}\,\sqrt{\xi\eta}\,e^{\pm i\phi} \equiv \Psi_{2\pm},\\
\Psi_{1,0,0} &= 8^{-1}\pi^{-1/2}\,e^{-(\xi+\eta)/4}\,(\xi - 2) \equiv \Psi_3,
\end{aligned} \tag{9}$$

and we will use the simplified notation on the right.

Among the quantum numbers $n, m, n_A, n_\xi, n_\eta, h, k, H$, and K, only three are independent. Besides Eqs. (8) we have $n_\xi = \inf(h,k)$, $n_\eta = \inf(H,K)$, $h - k = H - K = m$, $h + K = k + H = N \equiv n - 1$. We will often use N for $n - 1$ in our formulas. At fixed n we choose $\{h,k\}$ as independent numbers, represent a Stark state by a point $\mathbf{M} = (h,k)$ in a square $n \times n$ lattice, as shown in Fig. 2, and use the notation $|h,k\rangle$ or $|\mathbf{M}\rangle$ for $|n_\xi,n_\eta,m\rangle$. The Stark shifts of $\mathcal{E}$, λ, and μ at LO are

$$\begin{aligned}
\delta\mathcal{E}_\mathbf{M} &= n_A\,\omega_S\,, \quad \omega_S = 3Fn/2\,,\\
\delta\lambda_\mathbf{M} &= +Fn^3\,[3(\lambda^{(0)})^2 - m^2 + 1]/4\,,\\
\delta\mu_\mathbf{M} &= -Fn^3\,[3(\mu^{(0)})^2 - m^2 + 1]/4\,.
\end{aligned} \tag{10}$$

The lattice corners $h = k = 0$ and $H = K = 0$ represent the short-lived "red" and long-lived "blue" states. Their classical limits at large n are *linear* Kepler orbits of eccentricity

[2] We use atomic units (a.u.). For time and electric and magnetic fields, they are 2.42×10^{-17} s, 5.14×10^9 V/cm, and 2.35×10^5 Tesla.

[3] Following the usual convention, ξ and η are, respectively, the "uphill" and "downhill" coordinates. However, our z axis is in the downhill direction.

[4] $(\check{x},\check{y},\check{X},\check{Y}) = \nu^{-1/2}(u_3,u_4,u_1,u_2)$ of Ref. [18].

[5] λ and μ are twice α_1 and α_2 of Ref. [2] or β_1 and β_2 of Ref. [3].

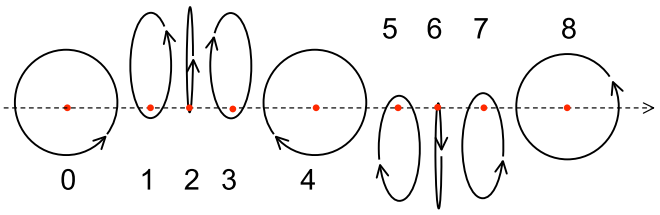

FIG. 3. Classical picture of the Stark oscillations of L_y and A_x. Orbits 0 to 7 correspond to the eight panels of Fig. 4.

$e_{cc} = 1$, like orbits 2 and 6 in Fig. 3. At the two other corners we have the *circular* states orbiting in the (x,y) plane.

For $F = 0$ the *Runge-Lenz-Pauli vector*

$$\mathbf{A} = (-2\mathcal{H}_0)^{-1/2}\,[-\mathbf{r}/r + (\mathbf{p}\times\mathbf{L} - \mathbf{L}\times\mathbf{p})/2] \tag{11}$$

is conserved. Stark states are $A_z = n_A$ eigenstates. At fixed n,

$$\mathbf{A}\cdot\mathbf{L} = 0, \quad \mathbf{A}^2 + \mathbf{L}^2 = n^2 - 1, \tag{12}$$

and $\langle\mathbf{r}\rangle = -3n\langle\mathbf{A}\rangle/2$.[6] The *pseudospins* $\mathbf{j}_1 = (\mathbf{L}+\mathbf{A})/2$ and $\mathbf{j}_2 = (\mathbf{L}-\mathbf{A})/2$ obey the usual spin commutations rules $\mathbf{j}\times\mathbf{j} = i\,\mathbf{j}$ and $\mathbf{j}^2 = j(j+1)$, with $j \equiv N/2$.

Superposition of **E** *and* **B** *fields.* To first order in **E** and **B** the perturbation Hamiltonian restricted to the n manifold is

$$\mathcal{H}_I = \boldsymbol{\omega}_S\cdot\mathbf{A} + \boldsymbol{\omega}_L\cdot\mathbf{L} = \boldsymbol{\omega}_1\cdot\mathbf{j}_1 + \boldsymbol{\omega}_2\cdot\mathbf{j}_2, \tag{13}$$

with $\boldsymbol{\omega}_S = -(3n/2)\mathbf{E}$, $\boldsymbol{\omega}_L = \mathbf{B}/2$, and $\boldsymbol{\omega}_{1,2} = \boldsymbol{\omega}_L \pm \boldsymbol{\omega}_S$. The stationary states are labeled by the pseudomagnetic quantum numbers[7]

$$i_\alpha \equiv \mathbf{j}_\alpha\cdot\hat{\boldsymbol{\omega}}_\alpha \quad (\alpha = 1,2). \tag{14}$$

In the electric field $-F\hat{\mathbf{z}}$, $i_1 = j_{1,z} = h - j = (n_A + m)/2$ and $i_2 = -j_{2,z} = k - j = (n_A - m)/2$, as indicated in Fig. 2. This figure also applies to general {**E**,**B**} configurations, but the quantification axes $\hat{\boldsymbol{\omega}}_1$ and $\hat{\boldsymbol{\omega}}_2$ for $\mathbf{j}_1$ and $\mathbf{j}_2$ may be at an angle. The energy shifts $\delta\mathcal{E} = |\boldsymbol{\omega}_1|\,i_1 + |\boldsymbol{\omega}_2|\,i_2$ are usually nondegenerate. For nonstationary states the expectation values of **A**, **L**, $\mathbf{j}_1$, and $\mathbf{j}_2$ obey the secular equations (see, e.g., [2,21,22])

$$\begin{aligned} d\bar{\mathbf{A}}/dt &= \boldsymbol{\omega}_L\times\bar{\mathbf{A}} + \boldsymbol{\omega}_S\times\bar{\mathbf{L}}\,,\\ d\bar{\mathbf{L}}/dt &= \boldsymbol{\omega}_S\times\bar{\mathbf{A}} + \boldsymbol{\omega}_L\times\bar{\mathbf{L}}\,, \end{aligned} \tag{15}$$

$$d\,\bar{\mathbf{j}}_\alpha/dt = \boldsymbol{\omega}_\alpha\times\bar{\mathbf{j}}_\alpha \quad (\alpha = 1,2). \tag{16}$$

Coherent elliptic states. These states are quasiclassical states (see, e.g., [22,23] and references therein) fully defined by their expectation values $\bar{\mathbf{A}}$ and $\bar{\mathbf{L}}$ of **A** and **L**, with the constraint

$$\bar{\mathbf{A}}\cdot\bar{\mathbf{L}} = 0\,, \quad \bar{\mathbf{A}}^2 + \bar{\mathbf{L}}^2 = N^2 \tag{17}$$

[compare with (12)]. We denote them as $|\bar{\mathbf{A}},\bar{\mathbf{L}}\rangle$. For the pseudospins,

$$|\bar{\mathbf{j}}_1| = |\bar{\mathbf{j}}_2| = j \equiv N/2\,. \tag{18}$$

The circular (linear) states are obtained for $\bar{\mathbf{j}}_1 = \bar{\mathbf{j}}_2$ ($\bar{\mathbf{j}}_1 = -\bar{\mathbf{j}}_2$). If $\bar{\mathbf{j}}_1$ and $\bar{\mathbf{j}}_2$ make an angle 2α, the classical Kepler orbit has eccentricity $e_{cc} = |\bar{\mathbf{A}}|/N = \sin\alpha$. In a weak field {**E**,**B**} the CES character is preserved by the evolution (15) and (16). The stationary CESs have $\bar{\mathbf{j}}_1 = \pm j\,\hat{\boldsymbol{\omega}}_1$ and $\bar{\mathbf{j}}_2 = \pm j\,\hat{\boldsymbol{\omega}}_2$. They sit at the corners of the (i_1,i_2) lattice associated with {**E**,**B**}. Their Kepler orbits are elliptic for noncolinear **E** and **B**.

CESs expand in the Stark basis as follows (see Appendix A):

$$|\bar{\mathbf{A}},\bar{\mathbf{L}}\rangle = \sum_{\mathbf{M}} c_{\mathbf{M}}(\bar{\mathbf{A}},\bar{\mathbf{L}})\,|\mathbf{M}\rangle, \tag{19}$$

$$c_{\mathbf{M}}(\bar{\mathbf{A}},\bar{\mathbf{L}}) = \left[B_N^h(\bar{h}/N)\,B_N^k(\bar{k}/N)\right]^{1/2} e^{-ih\beta_1 + ik\beta_2}\,, \tag{20}$$

where β_1 and β_2 are the azimuths of $-\bar{\mathbf{j}}_1$ and $+\bar{\mathbf{j}}_2$, respectively, $\bar{h} = (N + \bar{A}_z + \bar{L}_z)/2$, $\bar{k} = (N + \bar{A}_z - \bar{L}_z)/2$, and $B_N^p(x) = \binom{N}{p} x^p\,(1-x)^{N-p}$ is the binomial p distribution of barycenter $\bar{p} = xN$.

III. STATES FOR A [v,L,F] EXPERIMENT

We need an initial state with $\bar{\mathbf{L}}_T = (\bar{L}_x, \bar{L}_y) \neq 0$. In the field $-F\hat{\mathbf{z}}$ it is a nonstationary state, with $\bar{\mathbf{L}}$ changing according to (15). Two kinds of CES candidates are presented below.

(1) *Circular L_y eigenstates.* These correspond to circular orbits in the (x,z) plane and have $L_y = \pm N$. We denote them as $|Ly\pm\rangle$. Their wave functions,

$$\Psi_{Ly\pm} = [n^{n+1}\,N!\sqrt{\pi}]^{-1}\,(z \pm ix)^N\,e^{-r/n}\,, \tag{21}$$

decompose in Stark states (9) according to Eqs. (19) and (20) with $-\beta_1 = \beta_2 = \pm\pi/2$ and $\bar{h} = \bar{k} = N/2$. Therefore,

$$c_{\mathbf{M}}(Ly\pm) = (\pm i)^{h+k}\,2^{-N}\left[\binom{N}{h}\binom{N}{k}\right]^{1/2}. \tag{22}$$

At large n, $c_{\mathbf{M}}$ is important only near the center of the lattice. Indeed, $\bar{L}_z = \bar{A}_z = 0$, and the quantum fluctuations are $\langle m^2\rangle = \langle n_A^2\rangle = N/2 \ll N^2$. According to (15), the Kepler orbit changes continuously, as depicted in Fig. 3, keeping $\bar{A}_x^2 + \bar{L}_y^2 = N^2$ and $\bar{L}_x = \bar{L}_z = \bar{A}_y = \bar{A}_z = 0$. $\bar{L}_y$ and $\bar{A}_x$ oscillate in quadrature at the Stark frequency $\omega_S = 3nF/2$. Such oscillations have been observed with Stark *wave packets* [24]. The quasilinear orbits 2 and 6 in Fig. 3 correspond to the red and blue Stark states in an external field along $+\hat{\mathbf{x}}$. Since L_y oscillates, we can already infer that the [**v**,**L**,**F**] effect results in an oscillating $\langle v_x\rangle$.

Case with $n = 2$. Equations (9) and (21) give at $t = 0$

$$\Psi_{Ly\pm} = [\Psi_1 - \Psi_3 \pm i(\Psi_{2+} + \Psi_{2-})]/2\,. \tag{23}$$

Taking into account the Stark shifts (10), we have[8] at $t > 0$

$$\begin{aligned} \Psi(t) &= e^{it/8}[e^{i\omega_S t}\,\Psi_1 - e^{-i\omega_S t}\,\Psi_3 \pm i\,(\Psi_{2+} + \Psi_{2-})]/2 \qquad (24)\\ &= e^{it/8}[\cos^2(\omega_S t/2)\,\Psi_{Ly\pm} - \sin^2(\omega_S t/2)\,\Psi_{Ly\mp}\\ &\quad + (i/\sqrt{2})\sin(\omega_S t)\,\Psi_{2s}], \qquad (25) \end{aligned}$$

[6] In the quantum approach $\langle\mathcal{O}\rangle$ or $\overline{\mathcal{O}}$ is the expectation value of an observable $\mathcal{O}$. In the classical approach it is its average during one orbital revolution.

[7] Vectors with a hat are unitary; $\hat{\mathbf{X}} \equiv \mathbf{X}/|\mathbf{X}|$ for any vector **X**.

[8] $\Psi(t)$ is a shorthand notation for $\Psi(t,x,y,z)$ or $\Psi(t,\mathbf{r})$. When the argument t is omitted, Ψ designates the wave function at $t = 0$: $\Psi(\mathbf{r}) \equiv \Psi(0,\mathbf{r})$.

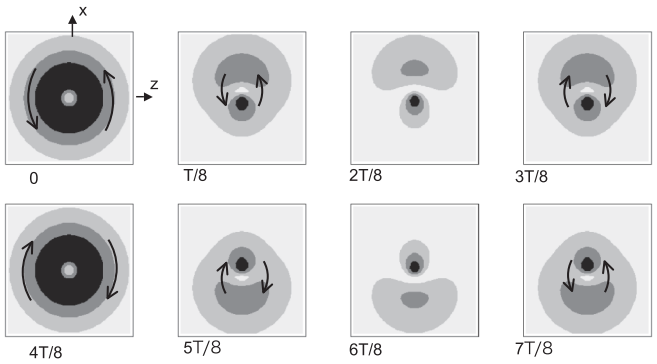

FIG. 4. Evolution of the electron density $|\Psi(t,\mathbf{r})|^2$ of Eqs. (24) and (25) ($y=0$ slice) during one Stark period T_S. At $4t/T_S = 0,1,2,3,4$, $\Psi(t)$ takes the values Ψ_{Ly+}, $i\Psi_{x+}$, $-\Psi_{Ly-}$, $-i\Psi_{x-}$, and Ψ_{Ly+} again, where $\Psi_{x\pm}$ is the $A_x = \pm 1$ eigenstate. Ψ vanishes along the current vortex $z=0$, $2 \pm x/\sin(3Ft) = r$ (whirling as indicated by arrows). For $t = T_S/4$ or $3T_S/4$, Ψ vanishes on the surface $2 \pm x = r$. The x and z windows are $[-7,+7]$.

where $\Psi_{2s} = (32\pi)^{-1/2}(r-2)e^{-r/2}$ is the $2S$ wave function. Thus the atom oscillates between three L_y eigenstates with the Stark period $T_S = 2\pi/\omega_S$. A complete oscillation of $\Psi(t,x,y,z)$ is analyzed in Fig. 4.

(2) *Rotating oblique elliptic states.* For a CES $|\bar{\mathbf{A}},\bar{\mathbf{L}}\rangle$ of *oblique* $\bar{\mathbf{L}}$ (i.e., both $\bar{\mathbf{L}} \times \mathbf{F}$ and $\bar{\mathbf{L}} \cdot \mathbf{F} \neq 0$), the evolution of the Kepler orbit differs from that in Fig. 3: since $\langle m \rangle \equiv \bar{\mathbf{L}} \cdot \hat{\mathbf{F}}$ is conserved, $\bar{\mathbf{L}}$ never vanishes, and linear states are avoided. An example is given in [25]. The advantage is a longer radiative lifetime and, for nonhydrogenic atoms, a strong reduction of core effects. In fact, noncircular elliptic states contain components of any l, but the low-l ones are negligible if $|\bar{\mathbf{L}}| \gg \sqrt{n}$. Let $P(l)$ be the total weight of the l components. For $|\bar{\mathbf{L}}| \sim \sqrt{n}$, Eq. (12) of Ref. [26] gives, for instance,

$$P(0) = n^{-1}\, e_{cc}^{2n-2} \sim n^{-1}\, e^{-\bar{\mathbf{L}}^2/N}\,,$$
$$P(1) = 3(n-1)(n+1)^{-1}\,(2e_{cc}^{-2}-1)\,P(0)\,, \qquad (26)$$

with $e_{cc} = (1 - \bar{\mathbf{L}}^2/N^2)^{1/2}$ being the eccentricity. The ROE states are CESs with either $\bar{\mathbf{j}}_1$ or $\bar{\mathbf{j}}_2$ parallel to $\mathbf{E}$. Then the ellipse rotates rigidly about $\mathbf{E}$ at angular velocity ω_S, with $\bar{\mathbf{L}}$ and $\bar{\mathbf{A}}$ being oblique and coplanar with $\mathbf{E}$ (see Fig. 5). The coefficients $c_{\mathbf{M}}$ of (19) are nonzero only on one border of the

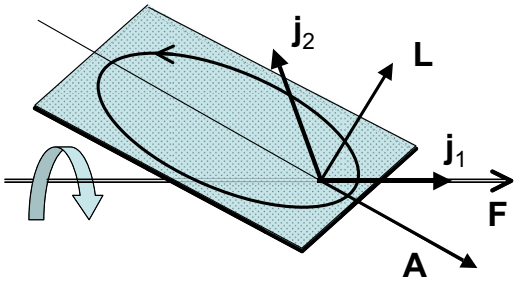

FIG. 5. Classical orbit of a ROE state. The orbit plane rotates as indicated by the curved arrow. The overbar of $\bar{\mathbf{j}}$, $\bar{\mathbf{L}}$, and $\bar{\mathbf{A}}$ has been omitted.

$\{h,k\}$ lattice. Equation (20) simplifies into

$$c_{\mathbf{M}}(\bar{\mathbf{A}},\bar{\mathbf{L}}) = \left[B_N^h(\bar{h}/N)\right]^{1/2} e^{-im\beta} \times (\delta_{k,0} \text{ or } \delta_{k,N}) \qquad (27)$$

or the same expression with $h \leftrightarrow k$. β is the azimuth of $-\bar{\mathbf{A}}$ at $t=0$. The example in Fig. 5, with $\bar{\mathbf{j}}_1 = j\,\hat{\mathbf{z}}$, corresponds to the choice with a $\delta_{h,N}$ factor. The fact that (27) contains n instead of n^2 terms is a big simplification. Since the ellipse is precessing about $\mathbf{E}$, we can already infer that the mean transverse velocity $\langle \mathbf{v}_T \rangle$ due to the $[\mathbf{v},\mathbf{L},\mathbf{F}]$ effect is *rotating* about $\mathbf{E}$.

Case with $n=2$. The four kinds of ROE states are given by

$$e^{-it/8}\,\Psi(t) = \sin\alpha\,\Psi_1\,e^{+i\omega_S t} + e^{\mp i\beta}\,\cos\alpha\,\Psi_{2\pm} \qquad (28a)$$

or

$$e^{-it/8}\,\Psi(t) = \sin\alpha\,\Psi_3\,e^{-i\omega_S t} + e^{\mp i\beta}\,\cos\alpha\,\Psi_{2\pm}, \qquad (28b)$$

where $\sin\alpha = e_{cc}$. The Ψ_3, Ψ_{2+} mixture is of the type shown in Fig. 5.

IV. PREPARATION OF CLy AND ROE STATES

In this section we consider only the case $n \gg 1$, where the necessary field for ionization is technically obtainable. As readily visible in Eq. (19), circular CLy and ROE states are coherent superposition of eigenstates of all $|m| \leqslant N$. Therefore their production is not trivial. Indeed, in a static electric field an optical transition from a low excited state will populate only low $|m|$ values (typically, $|m| = 0$, 1 or 2). Nevertheless, several methods [22,23,27–31] exist to produce circular or elliptic states. Let us recall the general principle of one of them [23,29,31] in the hydrogenic case. It can be schematically decomposed in two or three steps: (I) *optical excitation*, in a field $\mathbf{E}_0$, from the ground state to the red or blue linear Stark state of the nth shell, $|\bar{\mathbf{A}},0\rangle$ with $\bar{\mathbf{A}} = \pm N\,\hat{\mathbf{E}}_0$, (II) *circularization* of this state, changing $\mathbf{E}_0$ into a time-dependent field $\mathbf{E}(t)$ plus optionally a magnetic field $\mathbf{B}(t)$, and (III) *setting up the final field* $\{\mathbf{E},\mathbf{B}\}$ (if not already done in step II). An example is the setting of the final electric field shown in Fig. 1(d) of [29].

For step II, Ref. [23] proposes a constant $\mathbf{B}$ plus a slowly decreasing $\mathbf{E}(t)$. Reference [22] proposes a rotating $\mathbf{E}(t)$. Another possibility is suggested by Fig. 3: starting from linear orbit 2, created in a field $\mathbf{E}_0 \parallel \hat{\mathbf{x}}$, one can first turn off $\mathbf{E}_0$, then turn on a field $\mathbf{E}$ in the $-\hat{\mathbf{z}}$ direction. After a 1/4 Stark period circular state 4 is obtained and should remain like this if $\mathbf{E}$ is turned off. These changes must satisfy adiabatic conditions discussed below. Infinitely many other field configurations can realize step II. It suffices to choose two independent paths $\bar{\mathbf{j}}_1(t)$ and $\bar{\mathbf{j}}_2(t)$ on the sphere of radius j from the initial $\bar{\mathbf{j}}_1$ and $\bar{\mathbf{j}}_2$ to the wanted final ones. Inverting (16), we get

$$\boldsymbol{\omega}_i(t) = [\bar{\mathbf{j}}_i \times d\,\bar{\mathbf{j}}_i/dt]\,/j^2 + f_i(t)\,\bar{\mathbf{j}}_i(t) \quad (i=1,2)\,, \qquad (29)$$

with f_1 and f_2 being arbitrary functions. The needed fields are $\mathbf{E}(t) = [\boldsymbol{\omega}_2(t) - \boldsymbol{\omega}_1(t)]/(3n)$, $\mathbf{B}(t) = \boldsymbol{\omega}_1(t) + \boldsymbol{\omega}_2(t)$. One can do without magnetic field and use rotating electric fields; in the rotating frame the Coriolis force acts as a magnetic field. Figure 6 shows how to produce a ROE state in this way.

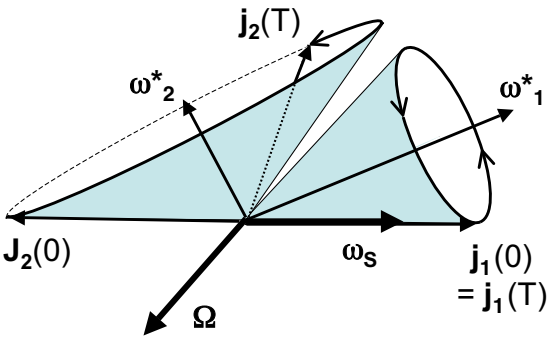

FIG. 6. Construction of a ROE state. At $t < 0$ the external field $\mathbf{E} = \mathbf{E}_0$ is static, and the atom is in the blue Stark state: $\bar{\mathbf{j}}_1(0) = -\bar{\mathbf{j}}_2(0) = j\hat{\boldsymbol{\omega}}_S(0)$, where $\boldsymbol{\omega}_S(t) \equiv -(3n/2)\mathbf{E}(t)$. During the interval $[0,T]$ one makes $\mathbf{E}$ rotate about $\boldsymbol{\Omega}$. The figure shows what happens in the rotating frame: $\boldsymbol{\omega}_S$ is fixed, and the Coriolis force makes $\bar{\mathbf{j}}_1$ and $\bar{\mathbf{j}}_2$ rotate about $\boldsymbol{\omega}_1^* = -\boldsymbol{\Omega} + \boldsymbol{\omega}_S$ and $\boldsymbol{\omega}_2^* = -\boldsymbol{\Omega} - \boldsymbol{\omega}_S$, respectively. We choose $T = 2\pi/\omega_1^*$ and $\omega_2^* < \omega_1^*$, so that $\bar{\mathbf{j}}_1(T)$ has rejoined $j\hat{\boldsymbol{\omega}}_S(T)$ while $\bar{\mathbf{j}}_2(T)$ had not yet rejoined $-j\hat{\boldsymbol{\omega}}_S(T)$. At $t > T$ the field is static again: $\mathbf{E} = \mathbf{E}(T)$. The atom is then in a ROE state where $\bar{\mathbf{j}}_1(t) = j\hat{\boldsymbol{\omega}}_S(T)$ and $\bar{\mathbf{j}}_2(t)$ starts rotating about $-\boldsymbol{\omega}_S(T)$. The overbar of $\bar{\mathbf{j}}_1$ and $\bar{\mathbf{j}}_2$ has been omitted.

Timing. The state we need for the $[\mathbf{v},\mathbf{L},\mathbf{F}]$ asymmetry is not stationary and starts to oscillate or rotate already during step III. We must know the values of $\bar{\mathbf{A}}$ and $\bar{\mathbf{L}}$ at the time ($t = 0$) when the measurement begins. They can, in principle, be calculated knowing $\{\mathbf{E}(t),\mathbf{B}(t)\}$ of step III.

Conditions to remain in the n manifod. To prevent inter-manifold (or δn) transitions during steps II and III, we require that the classical energy change of the electron matches the adiabatic energy change of the CES state with an error less than[9] $1/n^3$. The classical energy varies at the rate

$$\dot{\mathcal{E}}_{\rm cl}(t) = -\dot{\mathbf{F}}(t)\cdot\mathbf{r}(t) + (1/2)\,\dot{\mathbf{B}}(t)\cdot\bar{\mathbf{L}}(t) \tag{30}$$

(a dot means time derivative), whereas the adiabatic rate is

$$\dot{\mathcal{E}}_{\rm ad}(t) = (3n/2)\,\dot{\mathbf{F}}(t)\cdot\bar{\mathbf{A}}(t) + (1/2)\,\dot{\mathbf{B}}(t)\cdot\bar{\mathbf{L}}(t)\,. \tag{31}$$

Thus we require

$$\left|\int_{\text{step II}} dt\,\dot{\mathbf{F}}(t)\cdot[\mathbf{r}(t) + (3n/2)\,\mathbf{A}(t)]\right| < 1/n^3\,. \tag{32}$$

Due to $\langle\mathbf{r}\rangle = -3n\langle\mathbf{A}\rangle/2$ the integral over one Kepler period $T_K = 2\pi n^3$ almost vanishes when $\dot{\mathbf{F}}$ is nearly constant during this period. Only variations of $\dot{\mathbf{F}}(t)$ on smaller time scales may produce δn transitions, as expected from a quantum-mechanical treatment.

For nonhydrogenic atoms, δn transitions may also be produced by the *avoided crossings* [16,33,34] occurring at $|\mathbf{E}| \geqslant 1/(3n^5)$. These come from the non-Coulomb part of the potential and are no longer effective as soon as the CES has gained enough circularity in step II. Avoided crossings are useful in other methods, e.g., in [35].

[9]This is the spacing between states of adjacent n and close values of i_1 and i_2. Transitions between states of very different i_1 and i_2 are suppressed, as can be checked with Eqs. (42) and (43) of [32].

Preventing premature ionization. A last requirement is that the probability of tunneling ionization during step III remains small. $|\mathbf{E}(t)|$ must remain lower than $F_{\rm cr}(\mathbf{M})$ (defined in Sec. V) most of the time, at least for the states $|\mathbf{M}\rangle$ which contribute the most to (19). It must reach its final intensity F from below and not too slowly. Let $T_{\rm rise}$ be the rise time of $|\mathbf{E}(t)|$ from, say, $0.8\,F$ to F (due to the steep dependence of the Stark widths $\gamma_{\mathbf{M}}$ on F we can neglect tunneling below $0.8\,F$). We thus require $\gamma_{\mathbf{M}}\,T_{\rm rise} \ll 1$. On the other hand, (32) implies $T_{\rm rise} \gg T_K$. These two conditions are compatible if $\gamma_{\mathbf{M}}\,T_K \ll 1$. We *a priori* assume this last inequality: this means that the Stark resonance $|\mathbf{M}\rangle$ lives at least several Kepler periods.

Adiabatic versus diabatic steering inside the n manifold. Here adiabaticity [21] means that the atom can follow a quasistationary state (fixed i_1 and i_2) in the field $\{\mathbf{E}(t),\mathbf{B}(t)\}$. In particular the highest level stays the highest, and the lowest level stays the lowest. This requires the angular velocity of $\boldsymbol{\omega}_i(t)$ to be much smaller than $|\boldsymbol{\omega}_i|$:

$$|\dot{\boldsymbol{\omega}}_i \times \boldsymbol{\omega}_i| \ll |\boldsymbol{\omega}_i|^3 \quad (i = 1,2) \tag{33}$$

[see Eq. (10) of Ref. [23]]. Then, the evolution of the atom is tightly controlled, and the second term of (29) is dominant. For a CES this means that $\bar{\mathbf{j}}_1$ follows closely the vector $j\,\hat{\boldsymbol{\omega}}_1(t)$ or $-j\,\hat{\boldsymbol{\omega}}_1(t)$ and $\bar{\mathbf{j}}_2$ behaves similarly. A *diabatic* regime violates (33). It needs less field strength or field duration. In Ref. [29], step II [Fig. 1(b) of that work] is adiabatic but not step III [Fig. 1(d)]: when $B/E = 3n$, $\boldsymbol{\omega}_1$ or $\boldsymbol{\omega}_2$ crosses the origin, strongly violating (33). In our case step II or step III is necessarily diabatic since it transforms a stationary state into a nonstationary one.

We conclude from the above considerations that the preparation of a CLy or ROE state for a $[\mathbf{v},\mathbf{L},\mathbf{F}]$ experiment is possible, although not trivial.

V. TUNNELING FROM STARK STATES

For $F > 0$ the eigenstates of $\mathcal{H}$ are bound states in ξ and continuous *scattering states* in η, with both incoming and outgoing asymptotic waves. Up to a *critical field* $F_{\rm cr}(n,n_\xi,n_\eta)$ a Stark state is a *resonance* which can decay only by tunneling ionization. For $F > F_{\rm cr}$ the electron can escape classically. The position and wave function of a resonance may be obtained by looking for a bound-state solution of (4a) and solving (4b) semiclassically for $\check{R}$ below the return point. λ, μ, and ν are thus given by the equations $\lambda = \lambda(\nu^3 F; m, n_\xi)$, $\mu = \mu(\nu^3 F; m, n_\eta)$, and $\lambda + \mu = 2\nu$. $F_{\rm cr}$ is such that μ equals the potential barrier of (4b), $[\check{R}^2 - \nu^3 F\,\check{R}^4 + (m^2 - 1/4)/\check{R}^2]/2$, including the centrifugal term. Neglecting the latter and taking the unperturbed values (8) for μ and ν, we get the approximate *critical* field $F_{\rm cr}^{(0)}$ and *mean critical* field $\bar{F}_{\rm cr}^{(0)}$,

$$F_{\rm cr}^{(0)} = [8n^3(n - n_A)]^{-1}, \quad \bar{F}_{\rm cr}^{(0)} = 1/(8n^4)\,. \tag{34}$$

$F_{\rm cr}^{(0)}$ underestimates $F_{\rm cr}$. For $n \gg |m| + 1$, Eqs. (2.65) and (2.69) of [2] yield

$$n^3 F_{\rm cr}^{(0)}\big/(\nu^3 F_{\rm cr}) = \mu(F_{\rm cr})/\mu^{(0)} = 3\pi/\sqrt{128} \simeq 5/6\,. \tag{35}$$

As in [3,6], we describe Stark resonances as discrete states of complex energy $\mathcal{E} = \epsilon_R - i\gamma/2$, which contain only the outgoing asymptotic wave: the GS states [36,37]. To calculate

their widths or *decay rates* γ one needs only the *modulus* of the asymptotic Gamow-Siegert wave function $\Psi_{\rm GS}$. Since we are interested in the ionization of CLy or ROE states, which are linear combination of Stark states, we also need the *relative phases* of the asymptotic $\Psi_{\rm GS}$. Below we briefly summarize the semiclassical calculation of the widths and relative phases at LO (details are given in Appendix B).

The perturbation of $\chi(\xi)$ by $\mathbf{E}$ is neglected. Tunneling in η is calculated in the semiclassical approximation [1],

$$\Theta_{\rm GS}(\eta) \simeq \Theta_{\rm GS}(\eta_0)[p_\eta(\eta_0)/p_\eta(\eta)]^{1/2} e^{S(\eta_0,\eta)}\,, \tag{36}$$

$$S(\eta_0,\eta) = i\int_{\eta_0}^{\eta} p_\eta(s)\,ds\,, \tag{37}$$

with $p_\eta^2(\eta) = \mathcal{E}/2 + (1-m^2)/\eta^2 + Z_\eta/\eta + F\eta/4$. Equation (36) can be extended in the complex η plane and is valid for η and η_0 far enough from the tunnel entrance and exit, $\eta_{\rm in}$ and $\eta_{\rm ex}$, where $p_\eta^2 = 0$. We chose η_0 inside the tunnel (the classically forbidden region) such that

$$\eta_{\rm in} \ll \eta_0 \ll \eta_{\rm ex}\,, \quad |S(\eta_{\rm in},\eta_0| \gg 1\,, \quad |S(\eta_0,\eta_{\rm ex}| \gg 1. \tag{38}$$

These conditions can easily be met if $F \ll F_{\rm cr}^{(0)}$. A natural choice is $\eta_0 = (\eta_{\rm in}\,\eta_{\rm ex})^{1/2}$, where $-p_\eta^2$ is nearly maximum. In (36) $\Theta_{\rm GS}(\eta_0)$ is approximated by the unperturbed Stark wave function $\Theta_{\rm St}(\eta_0)$. The integration of (37) is done along a path in the upper complex half plane, avoiding cuts of $p_\eta(s)$. The result for (36) is independent of the precise choice of η_0. The knowledge of the behavior of $\Theta_{\rm GS}(\eta)$ near $\eta_{\rm ex}$ is not needed (it is a combination of Ai and Bi functions; see, e.g., Ref. [4(b)]).

The width. Equations (B4) and (B5) of Appendix B give

$$\gamma_{\mathbf{M}} = \left(\frac{4}{F\nu^3}\right)^{\mu} \exp\left(-\frac{2}{3F\nu^3}\right)\frac{\nu^{-3}}{H!\,K!}\,, \tag{39}$$

in accordance with Eq. (125) of [3]. At LO we replace μ with $\mu^{(0)} = n - n_{\rm A}$ and ν with n, except in the exponential where $\nu^{-3} \simeq n^{-3} - 9Fn_{\rm A}/2$. One gets the Slavjanov result [38] [see also [4] and Eq. (2.80) of [2] and Eq. (126) of [3]]:

$$\gamma_{\mathbf{M}} = \left(\frac{4}{Fn^3}\right)^{n-n_{\rm A}} \exp\left\{3n_{\rm A} - \frac{2}{3Fn^3}\right\}\frac{n^{-3}}{H!\,K!}$$
$$= \gamma_{\rm min}\,(f^{-H}/H!)\,(f^{-K}/K!). \tag{40}$$

$f \equiv Fn^3e^3/4$ and $\gamma_{\rm min} = (n^3 f)^{-1}\,\exp\{3n - 2/(3Fn^3)\}$ is the width of the blue state $n_{\rm A} = n-1$. For the $n=2$ states (9),

$$\gamma_2 = 2^{-5}F^{-2}\,e^{-1/(12F)}\,,$$
$$\gamma_3/\gamma_2 = \gamma_2/\gamma_1 = 2Fe^3\,. \tag{41}$$

Let us also mention an approximate intuitive formula for the width:

$$\gamma = T_\eta^{-1}\,\exp\{-2S(\eta_{\rm in},\eta_{\rm ex})\}\,, \tag{42}$$

where T_η is the classical period of the η motion. See Eq. (2.73) of [2], Eq. (63) of [39], and Eq. (7.9) of [8].

The asymptotic Gamow-Siegert wave function. The η-dependent phase is given by the second line of Eq. (B4). Replacing $\mathcal{E}$ with $-1/(2n^2) + \delta\mathcal{E} - i\gamma/2$ in (B4) and $\check{\chi}$ in (6) with $\Phi_{h,k}$ and including the time dependence gives

$$\Psi_{\rm GS}(t,\mathbf{r}) \sim \exp\{it/(2n^2)\}\,U(t^*,\check{x},\check{y})\,V(\eta)\,, \tag{43}$$

$$U(t^*,\check{x},\check{y}) = i^\mu\sqrt{\gamma}\,\exp\{-(\gamma/2 + i\delta\mathcal{E})t^*\}\,\Phi_{h,k}(\check{x},\check{y}), \tag{44}$$

$$V(\eta) = \sqrt{i}\,(Fn^2\eta^3)^{-1/4}\,\exp\{i(\eta-\bar\eta_{\rm ex})^{3/2}\sqrt{F}/3\}. \tag{45}$$

$\bar\eta_{\rm ex} = 1/(Fn^2)$ is the tunnel exit for $n_{\rm A} = 0$ and $|m| = 1$; $t^* = t - [(\eta-\bar\eta_{\rm ex})/F]^{1/2}$ is the classical time at which the electron exits the tunnel if it reaches point η at time t (it is analogous to the retarded time in classical radiation theory). The exponential of (44) takes into account the energy shift and the decay of the wave. $V(\eta)$ is common to the n manifold.

Note that once the external field $\mathbf{E}$ is switched on, the transition from a Stark wave function $\Psi_{\rm St}(t,\mathbf{r})$ to a Gamow-Siegert wave function $\Psi_{\rm GS}(t,\mathbf{r})$ is not instantaneous. At large η, due to the finite velocity of the electron, the Gamow-Siegert wave function sets up only when t^* becomes positive.

$|\Psi_{\rm GS}(t,\mathbf{r})|^2$ of (43)–(45) can be roughly interpreted as the density of a classical electron cloud falling freely in the uniform force field $\mathbf{F}$. An electron of this cloud which leaves the tunnel at time t^* follows approximately a parabolic motion $z = \bar\eta_{\rm ex}/2 + (t-t^*)^2F/2 = (x/\check{x})^2/(2n) = (y/\check{y})^2/(2n)$, with fixed parameters $\check{x}$ and $\check{y}$. Its transverse velocity $\mathbf{v}_{\rm T} \simeq (\check{x},\check{y})\sqrt{nF}$ gives access to $|\check{\chi}(\check{x},\check{y})|^2$ in the imaging method of [7–11].

The i^μ factor in Eq. (44) plays an essential role in the $[\mathbf{v},\mathbf{L},\mathbf{F}]$ effect. It yields the relative phase between different GS asymptotic wave functions. We recall that the above calculations are made at lowest order in F. When $F \sim F_{\rm cr}^{(0)}$, they become inaccurate [see condition (48) of [4(b)]], even in order in magnitude, because the errors of $S(\eta_0,\eta)$ are amplified by the exponentiation in (36).

VI. TUNNELING FROM A $\langle \mathbf{L}_{\rm T}\rangle \neq 0$ STATE

We assume that at $t = 0$ the atom has been prepared in a CLy or ROE state in the field $\mathbf{E} = -F\,\hat{\mathbf{z}}$, as discussed in Sec. IV. Then tunneling ionization begins together with oscillations or orbit precession about $\hat{\mathbf{z}}$. At large η its time-dependent wave function is obtained from (20) and (43)–(45):

$$\Psi(t,\mathbf{r}) \sim \exp\{it/(2n^2)\}\,V(\eta)\,\check{\psi}(t^*,\check{x},\check{y})\,, \tag{46a}$$

$$\check{\psi}(t^*,\check{x},\check{y}) = \sum_{\mathbf{M}} c_{\mathbf{M}}\,U_{\mathbf{M}}(t^*,\check{x},\check{y}). \tag{46b}$$

$|\check{\psi}(t^*,\check{x},\check{y})|^2$ may be measured with the imaging method of [7–11].

The $[\mathbf{v},\mathbf{L},\mathbf{F}]$ *asymmetry.* This asymmetry is related to the asymmetry of $|\check{\psi}(t^*,\check{x},\check{y})|^2$, recalling that $\mathbf{v}_{\rm T} \simeq (\check{x},\check{y})\sqrt{nF}$. A first measure of it is the mean transverse velocity $\bar v_{\rm T}$ of components

$$\bar v_x(t^*) = (nF)^{1/2}\,I_{\{x\}}(t^*)/I(t^*) \tag{47}$$

and similarly for $x \to y$. $I_{\{w\}}$ is defined for any function $w(\check{x},\check{y})$ by

$$I_{\{w\}}(t^*) \equiv \langle\check{\psi}(t^*,\check{x},\check{y})\,|w(\check{x},\check{y})|\,\check{\psi}(t^*,\check{x},\check{y})\rangle \tag{48}$$

and $I \equiv I_{\{1\}}$. We also define the alternative asymmetry parameters:

$$a_x(t^*) = \Delta_x I(t^*)/I(t^*)\,, \tag{49}$$

$$b_x(t^*) \equiv \bar{v}_x \big/ \langle v_x^2 \rangle^{1/2} = I_{\{x\}}(t^*)/\sqrt{I(t^*)\, I_{\{x^2\}}(t^*)}, \tag{50}$$

and similarly for $x \to y$. $\Delta_x I = I_{\{w\}}$ for $w = \mathrm{sgn}(\check{x})$. $\bar{v}_x$, a_x, and b_x give similar information, but $|a_x(t^*)|$ and $|b_x(t^*)|$ are bound by 1, while $\bar{v}_x$ is of the order of $(F/F_{\rm cr})^{1/2}\, n^{-1}$. $a_x(t^*)$ can be simply measured with two half-plane detectors.

A. Asymmetry for $n = 2$

The $n = 2$ case contains the basic features which remain at higher n. We treat it in detail for a CLy state and then mention the main changes for a ROE state. From Eqs. (46b), (44), and (22),

$$\begin{aligned}\check{\psi}(t^*,\check{x},\check{y}) = (1/2)\,\big\{ & i^{\mu_1}\sqrt{\gamma_1}\, e^{(-i\delta\mathcal{E}_1-\gamma_1/2)t^*}\,\Phi_{00} \\ & -i^{\mu_3}\sqrt{\gamma_3}\, e^{(-i\delta\mathcal{E}_3-\gamma_3/2)t^*}\,\Phi_{11} \\ & \pm i^{\mu_2+1}\sqrt{\gamma_2}\, e^{(-i\delta\mathcal{E}_2-\gamma_2/2)t^*}\,(\Phi_{10}+\Phi_{01})\big\}. \end{aligned} \tag{51}$$

Applying (7) and taking the square modulus,

$$\begin{aligned}|\check{\psi}(t^*,\check{x},\check{y})|^2 = (4\pi)^{-1}\, e^{-\check{x}^2-\check{y}^2}\big\{ & \gamma_1\, e^{-\gamma_1 t^*} + 4\gamma_2\, e^{-\gamma_2 t^*}\,\check{x}^2 \\ & + \gamma_3\, e^{-\gamma_3 t^*}\,(\check{x}^2+\check{y}^2-1)^2 \\ & \pm 4\sqrt{\gamma_1\gamma_2}\, e^{-\bar{\gamma}_{12} t^*}\,\check{x}\,\cos(\alpha_{12}-\omega_{12}t^*) \\ & \pm 4\sqrt{\gamma_2\gamma_3}\, e^{-\bar{\gamma}_{23} t^*}\,\check{x}\,(\check{x}^2+\check{y}^2-1)\,\cos(\alpha_{23}-\omega_{23}t^*) \\ & + 2\sqrt{\gamma_1\gamma_3}\, e^{-\bar{\gamma}_{13} t^*}\,\cos(\alpha_{13}-\omega_{13}t^*)\,(\check{x}^2+\check{y}^2-1)\big\}, \end{aligned} \tag{52}$$

where $\bar{\gamma}_{ij} \equiv (\gamma_i+\gamma_j)/2$, $\omega_{ij} \equiv \delta\mathcal{E}_i - \delta\mathcal{E}_j$, and $\alpha_{ij} \equiv (\delta\mu_i - \delta\mu_j)\,\pi/2$. To first order in F [see Eq. (10)],

$$\alpha_{12}/16 = \alpha_{23}/8 = \alpha_{13}/24 = -\pi F\,, \tag{53}$$

$$\omega_{12} = \omega_{23} = \omega_{13}/2 = -\omega_{\rm S} = -3F\,; \tag{54}$$

γ_i is given by (41) or, more accurately, by (39). The asymmetry comes from the odd part in $\hat{x}$. The quantities needed in (49) and (50) are obtained from (48) and (52):

$$4I = \gamma_1\, e^{-\gamma_1 t^*} + 2\gamma_2\, e^{-\gamma_2 t^*} + \gamma_3\, e^{-\gamma_3 t^*}, \tag{55a}$$

$$\Delta_x I = \pm\frac{1}{\sqrt{\pi}}\cos(\alpha_{12}-\omega_{12}t^*)\,\sqrt{\gamma_1\gamma_2}\, e^{-\bar{\gamma}_{12}t^*} \pm\frac{1}{2\sqrt{\pi}}\cos(\alpha_{23}-\omega_{23}t^*)\,\sqrt{\gamma_2\gamma_3}\, e^{-\bar{\gamma}_{23}t^*}, \tag{55b}$$

$$2I_{\{x\}} = \pm\cos(\alpha_{12}-\omega_{12}t^*)\,\sqrt{\gamma_1\gamma_2}\, e^{-\bar{\gamma}_{12}t^*} \pm\cos(\alpha_{23}-\omega_{23}t^*)\,\sqrt{\gamma_2\gamma_3}\, e^{-\bar{\gamma}_{23}t^*}, \tag{55c}$$

$$8I_{\{x^2\}} = \gamma_1\, e^{-\gamma_1 t^*} + 6\gamma_2\, e^{-\gamma_2 t^*} + 3\gamma_3\, e^{-\gamma_3 t^*} + 2\cos(\alpha_{13}-\omega_{13}t^*)\,\sqrt{\gamma_1\gamma_3}\, e^{-\bar{\gamma}_{13}t^*}. \tag{55d}$$

The time-dependent asymmetry. At LO, all cosines in (55b) and (55c) are equal to $\cos(\omega_{\rm S}t^*)$. $\bar{v}_x(t^*)$ oscillates at the Stark frequency and in phase[10] with $\langle L_y(t^*)\rangle$. When $\langle L_y\rangle > 0$, $\bar{v}_x > 0$, as guessed from Fig. 1. The outgoing electron stream is pictured in Fig. 7. If $\gamma_1 \gg \gamma_2 \gg \gamma_3$ (which is the case for $F \ll \bar{F}_{\rm cr}^{(0)}$), we can distinguish three "eras," depending on which term dominates in (55a). The transition between the ith and $(i+1)$th eras is at

$$t^*_{i,i+1} = (\gamma_i - \gamma_{i+1})^{-1}\,\ln[c_i\gamma_i/(c_{i+1}\gamma_{i+1})], \tag{56}$$

with $c_1 = c_3 = c_2/2 = 1$. At $t^*_{i,i+1}$ the Stark sublevels i and $i+1$ interfere with maximum efficiency. Let us denote by a° and v_x° the oscillation amplitudes of a_x and $\bar{v}_x$, obtained by replacing the $\pm$ cosine factors by $+1$ in (55b) and (55c). They have local maxima of heights $a^\circ(t^*_{1,2}) \simeq 2a^\circ(t^*_{2,3}) \simeq \sqrt{2/\pi}$ and $v_x^\circ(t^*_{1,2}) \simeq v_x^\circ(t^*_{2,3}) \simeq F^{1/2}$. Incidentally, $F^{1/2}$ is the transverse velocity $\langle L_y\rangle/z$ of the unperturbed CLy state at the saddle point $z = F^{-1/2}$. In the third era a° and v_x° fall off exponentially. Figure 8 plots $I(t^*)$ and $a^\circ(t^*)$ for $F = 0.004$, using the "exact" widths found in [4(a)].

The time-averaged asymmetry. Except for very small values of $F/\bar{F}_{\rm cr}^{(0)}$, $\bar{v}_x(t^*)$, $a_x(t^*)$, or $b_x(t^*)$ oscillates too fast to be

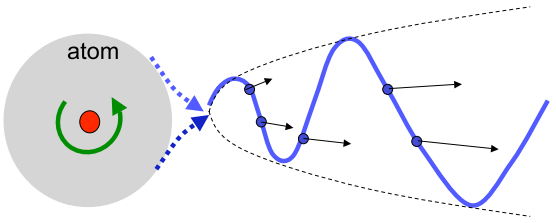

FIG. 7. Motion of the probability density $|\Psi(t,\mathbf{r})|^2$ of the outgoing electron. The curve represents $\langle x(t,z)\rangle \simeq 2\langle\check{x}(t)\rangle\sqrt{z}$ versus z at fixed t. With time, the undulations move to the right. It looks like a crawling snake.

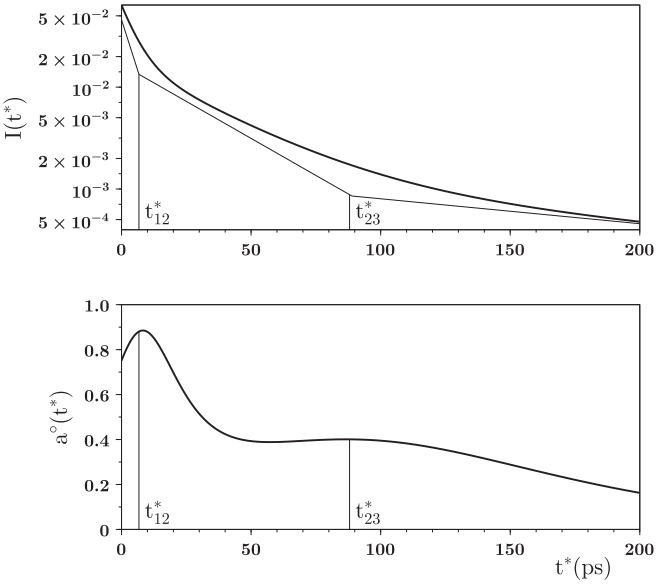

FIG. 8. Intensity $I(t^*)$ of the outgoing electron flux from an $n = 2$ CLy state [Eq. (55a)] and amplitude $a^\circ(t^*)$ of the oscillations of the asymmetry (49). The *time of exit* t^* is in picoseconds, and $I(t^*)$ is in ps^{-1}. Field intensity $F = 0.004$ a.u. The oscillations, of period $T_{\rm S} = 0.0127$ ps, are too dense to show. Note the change of "eras" and local maxima at $t^*_{1,2}$ and $t^*_{2,3}$. The sloping straight lines under the $I(t^*)$ curve represent the successive dominant contributions to (55a).

[10]It looks as if the group velocity is infinite in the tunnel.

TABLE I. Numerical results for the widths, the initial asymmetry, and the time-averaged asymmetry for the $n = 2$ CLy state. The "LO" results are at lowest order in F. The "corr." results are calculated with (39) with first-order corrections for μ and ν. The "num." results are based on numerical values of γ found in the literature.

$10^3 F$	Method	γ_1	γ_2	γ_3	$b_x(0)$	$a_x(0)$	$\langle b_x\rangle$
3.5	LO	8.3×10^{-7}	1.2×10^{-7}	1.6×10^{-8}	0.71	0.69	2.5×10^{-6}
	corr.	3.9×10^{-7}	7.7×10^{-8}	8.8×10^{-9}	0.75	0.75	1.4×10^{-6}
	num.[a]	3.9×10^{-7}	6.0×10^{-8}				
4.0	LO	1.1×10^{-5}	1.7×10^{-6}	2.8×10^{-7}	0.73	0.71	3.5×10^{-5}
	corr.	4.7×10^{-6}	1.1×10^{-6}	1.4×10^{-7}	0.77	0.78	1.9×10^{-5}
	num.[b]	4.4×10^{-6}	0.81×10^{-6}	1.4×10^{-7}			
5.0	LO	3.6×10^{-4}	7.2×10^{-5}	1.5×10^{-5}	0.75	0.75	1×10^{-3}
	corr.	1.3×10^{-4}	4.6×10^{-5}	6.2×10^{-6}	0.78	0.82	6.6×10^{-4}
	num.[c]	1.1×10^{-4}	2.6×10^{-5}	5.7×10^{-6}			
6.0	LO	0.0033	0.0008	0.0002	0.79	0.81	0.0049
	corr.	0.0011	0.00043	7.1×10^{-5}	0.78	0.83	0.0065
	num.[a]			6.1×10^{-5}			
6.5	LO	0.0077	0.0020	0.00052	0.77	0.78	0.052
8.0	LO	0.045	0.015	0.0047	0.81	0.85	0.28
	corr.	0.011	0.0066	0.0013	0.77	0.82	0.12
	num.[b]	0.0042	0.0020	0.00085			
10	LO	0.19	0.075	0.030	0.83	0.87	0.66
	corr.	0.032	0.029	0.0063	0.73	0.78	0.42
	num.[c]	0.011	0.0063	0.0033			

[a]Reference [[4](b)].
[b]Reference [[4](a)].
[c]Reference [6].

measured with an ordinary detector. For instance, $F > 0.002$ gives $T_S \lesssim 25$ fs. Therefore one can only measure the time-averaged asymmetry obtained by integrating $I_{\{w\}}(t^*)$. For instance,

$$\langle a_x\rangle = \int_0^\infty dt^*\, \Delta_x I(t^*) \tag{57}$$

[the integral of $I(t^*)$ is 1]. Integration of (55) is made using

$$\int_0^\infty dt^*\, e^{-\bar\gamma_{ij}t^*}\cos(\alpha_{ij}-\omega_{ij}t^*) = \frac{\bar\gamma_{ij}\,\cos\alpha_{ij}+\omega_{ij}\,\sin\alpha_{ij}}{\bar\gamma_{ij}^2+\omega_{ij}^2}. \tag{58}$$

If $\gamma_{ij} \ll \omega_{ij}$, the $\{ij\}$ contribution to the asymmetry is washed out by the oscillations of $I_{\{x\}}(t^*)$ or $\Delta_x I$. To get a sizable $\langle a_x\rangle$ one must take F such that the Stark oscillations are quenched by the decay of the Ψ_1 state, that is, $\gamma_1 \gtrsim \omega_S = 3F$.

Numerical results for $n = 2$ and discussion. Table I shows numerical results for the widths γ_i, the asymmetries a_x and b_x at $t^* = 0$, and the time average of b_x for seven values of F. For the largest F values we have $\gamma_1 > \omega_S$, Stark oscillations are quenched, and $\langle b_x\rangle$ is sizable. For $F > 0.005$ the widths given by Eq. (41) are much larger than the exact numerical results found in literature. Equation (39) gives better results, but again they are too big for $F \gtrsim 0.008$. In fact the chosen F are not small compared to $\bar F_{cr}^{(0)} = 0.0078$. Nevertheless, our main results concerning the asymmetry should be qualitatively true. First, the $[\mathbf{v},\mathbf{L},\mathbf{F}]$ asymmetry depends essentially on the ratios γ_1/γ_2 and γ_2/γ_3, which are not so badly predicted by (41). Second, widths not far from the exact ones are obtained if we replace F in Eq. (39) or (41) by a slightly reduced value. Compare, for instance, the exact results for $F = 0.008$ with the LO ones for $F = 0.0065$ or exact results for $F = 0.01$ with our "corr." ones for $F = 0.008$ in Table I. The smallness of this reduction is due to the very steep dependence of $\log\gamma$ on F. Note that the reduction from F_{cr} to $F_{cr}^{(0)}$ in Eq. (35) is of the same order.

Case of a ROE $n = 2$ state. The above calculations can be adapted to the ROE states (28) without great modifications. The following are the main changes:

(1) $\check\psi(t^*,\check x,\check y)$ involves two states instead of four in Eq. (51). In the analog of (52) $|\check\psi(t^*,\check x,\check y)|^2$ contains two γ_i terms and one $\sqrt{\gamma_i\gamma_j}$ term. We have two eras instead of three.

(2) $\Delta_y I(t^*)$ and $I_{\{y\}}(t^*)$ are nonzero and oscillate in quadrature with $\Delta_x I(t^*)$ and $I_{\{x\}}(t^*)$ such that $\langle\mathbf{v}_T\rangle$ rotates in the direct sense about $\hat{\mathbf{z}}$ for the Ψ_1,Ψ_{2+} and Ψ_3,Ψ_{2-} mixtures of (28) and in the retrograde sense for the two other mixtures. The undulating stream in Fig. 7 is replaced by a helical stream.

(3) The size of the asymmetry depends on the eccentricity $\sin\alpha$ and is bigger when the two components of (28a) or (28b) are comparable, i.e., $\alpha \simeq \pi/4$.

B. Asymmetry for large-*n* CESs

The $n = 2$ case was instructive, but the required field is not attainable in the laboratory. We therefore explore the large-n case, where the needed field ($\propto n^{-4}$ for $\mathbf{M}$ in the bulk of the $\{h,k\}$ lattice) is considerably reduced and experiments become feasible. Besides, the Stark period $T_S \sim n^3\times10^{-16}$ s can be long enough to make a time-resolved experiment possible. For instance, in [40] ($n \sim 20$) the escaping times of the electrons are recorded with a picosecond resolution. The $n = 2$ results generalize as follows:

Gathering (8), (10), (20), (44), (46b), and (48), we have, for a real function $w(\check{x},\check{y})$,

$$I_{\{w\}}(t^*) = \mathrm{Re}\sum_{\mathbf{M},\mathbf{M}'} i^{\mu-\mu'}\, c_{\mathbf{M}}\, c^*_{\mathbf{M}'}\, (\gamma_{\mathbf{M}}\gamma_{\mathbf{M}'})^{1/2} \times \exp(-\bar{\gamma}_{\mathbf{M}\mathbf{M}'}t^* - i\omega_{\mathbf{M}\mathbf{M}'}t^*)\,\langle\Phi_{h',k'}|w(\check{x},\check{y})|\Phi_{h,k}\rangle, \tag{59}$$

with $\bar{\gamma}_{\mathbf{M},\mathbf{M}'} = (\gamma_{\mathbf{M}} + \gamma_{\mathbf{M}'})/2$ and $\omega_{\mathbf{M},\mathbf{M}'} = \delta\mathcal{E}_{\mathbf{M}} - \delta\mathcal{E}_{\mathbf{M}'}$. The summation in (59) is restricted by *selection rules*. For I we have $\mathbf{M} = \mathbf{M}'$. For $I_{\{x\}}$ or $I_{\{y\}}$, $\mathbf{M}$ and $\mathbf{M}'$ are nearest neighbors: $|n'_{\mathrm{A}} - n_{\mathrm{A}}| = |m' - m| = 1$; the relevant matrix elements are

$$\langle\Phi_{h-1,k}|\check{x}|\Phi_{h,k}\rangle = -i\langle\Phi_{h-1,k}|\check{y}|\Phi_{h,k}\rangle = \sqrt{h}/2\,,$$
$$\langle\Phi_{h,k-1}|\check{x}|\Phi_{h,k}\rangle = +i\langle\Phi_{h,k-1}|\check{y}|\Phi_{h,k}\rangle = \sqrt{k}/2\,. \tag{60}$$

For $I_{\{x^2\}}$, $I_{\{y^2\}}$, or $I_{\{xy\}}$ we have $|n'_{\mathrm{A}} - n_{\mathrm{A}}| = |m' - m| = 0$ or 2. For $\Delta_x I$ or $\Delta_y I$ the only rule is $m - m'$ is an odd number. In the following we only consider the asymmetry parameters $\bar{v}_x \propto I_{\{x\}}$ and $\bar{v}_y \propto I_{\{y\}}$. We consider first a CLy state and then a ROE state.

Time-dependent asymmetry for a CLy state. The coefficients $c_{\mathbf{M}}$ are given by (22). The evaluation of (59) is simplified by the symmetry $\{h,h'\} \leftrightarrow \{k,k'\}$ of the $\mathbf{M}\mathbf{M}'$ contributions. Let us first examine the LO results.

At $t^* = 0$ all the contributions to $I_{\{x\}}$ have the same sign. Indeed, the matrix elements (60) of x are positive, and from (8) and (22), the argument of $i^{\mu-\mu'}c_{\mathbf{M}}c^*_{\mathbf{M}'}$ in (59) is $\alpha_{\mathbf{M}\mathbf{M}'} \equiv (\delta\mu - \delta\mu')\pi/2$ for the $|Ly+\rangle$ state and $\alpha_{\mathbf{M}\mathbf{M}'} + \pi$ for the $|Ly-\rangle$ state, and $\alpha_{\mathbf{M}\mathbf{M}'}$ is zero at LO. Thus the initial asymmetry is oriented as suggested by Fig. 1. Including the first-order correction does not change this result since $|\alpha_{\mathbf{M}\mathbf{M}'}| \simeq (3\pi/32)\,F/F^{(0)}_{\mathrm{cr}} < \pi/2$, from Eqs. (10) and (34). At $t^* > 0$, $\bar{v}_x(t^*)$ oscillates at the Stark frequency ω_{S}. A $\mathbf{M}\mathbf{M}'$ pair interferes with the maximum efficiency at

$$t^*_{\mathbf{M},\mathbf{M}'} = (\gamma_{\mathbf{M}} - \gamma_{\mathbf{M}'})^{-1}\,\ln[|c_{\mathbf{M}}|^2\gamma_{\mathbf{M}}/(|c_{\mathbf{M}'}|^2\gamma_{\mathbf{M}'})], \tag{61}$$

yielding a peak or at least a "knee" of the oscillation amplitude v°_x, like those of Fig. 8 for the $n = 2$ case. There are $n(n-1)$ such peaks. Most of them should not be discernible, and a subdivision in eras is less clear than in the $n = 2$ case. However, for $\mathbf{M}$ close to the $m = 0$ diagonal, $\gamma_{\mathbf{M}}$ and $|c_{\mathbf{M}}|$ depend mainly on n_{A}, with an approximate Gaussian dependence on m:

$$\gamma_{\mathbf{M}} \simeq \gamma_{\min}\sqrt{\frac{2/\pi}{N-n_{\mathrm{A}}}}\exp\left\{\frac{-m^2}{2(N-n_{\mathrm{A}})}\right\}\frac{(2/f)^{N-n_{\mathrm{A}}}}{(N-n_{\mathrm{A}})!}. \tag{62}$$

Therefore several $t^*_{\mathbf{M},\mathbf{M}'}$ almost coincide, making an enhanced peak.

The time-averaged asymmetry $\langle\bar{v}_x\rangle$. This asymmetry is obtained from (47) and (59) but replacing $I_{\{x\}}(t^*)$ by its time-integrated value and $I(t^*)$ by 1. The integration is made using (58) with $ij \to \mathbf{M}\mathbf{M}'$. To contribute significantly to $\langle\bar{v}_x\rangle$ a $\mathbf{M}\mathbf{M}'$ pair must fulfill $\sup(\gamma_{\mathbf{M}},\gamma_{\mathbf{M}'}) \gtrsim \omega_{\mathrm{S}}$ so that the Stark oscillation is quenched. It must also be near the center of the lattice of Fig. 2 to have a large enough $c_{\mathbf{M}}c^*_{\mathbf{M}'}$. For $|n_{\mathrm{A}}|$ and $|m| \ll \sqrt{n}$ the Stirling formula applied to (40) gives

$$\frac{\gamma_{\mathbf{M}}}{\omega_{\mathrm{S}}} \simeq \frac{8}{3\pi f'}\left(\frac{64e}{f'}\right)^{n-n_{\mathrm{A}}}\exp\left\{4n_{\mathrm{A}} - \frac{16n}{3f'} - \frac{n_{\mathrm{A}}^2+m^2}{2n}\right\}, \tag{63}$$

with $f' \equiv F/\bar{F}^{(0)}_{\mathrm{cr}} = 32\,e^{-3}\,nf$. Thus the oscillation quenching requires $\ln(64e/f') - 16/(3f') \gtrsim 0$, that is, $F \sim \bar{F}^{(0)}_{\mathrm{cr}}$ (we exclude the case $F > \bar{F}^{(0)}_{\mathrm{cr}}$).

Comparison between LO and exact γ *at large* n. We choose F not much smaller than $\bar{F}^{(0)}_{\mathrm{cr}}$ in order to get a large enough time-average asymmetry. As for $n = 2$, the Slavjanov formula (40) greatly overestimates the widths. Let us take, for instance, $n = 10$ and $F = 10^{-5}$. For $m = 1$ and $n_\xi = 4$, Table 5 of Ref. [5] gives $\gamma = 3.31\times10^{-12}$, whereas Eq. (40) gives $\gamma = 4.06\times10^{-10}$ (here $H = 5$, $K = 4$, and $n_{\mathrm{A}} = 0$). This is because F is not far from $F^{(0)}_{\mathrm{cr}} = 1.25\times10^{-5}$. Again, the correct result can be recovered with a small reduction of F ($F = 0.923\times10^{-5}$) in Eq. (40). Besides, the ratio $\gamma_{\mathbf{M}'}/\gamma_{\mathbf{M}}$ for neighboring $\mathbf{M}$ and $\mathbf{M}'$ is reasonably well described by Eq. (40). This is best seen when looking at $\hat{\gamma} \equiv H!\,K!\,\gamma$. According to (40), the ratio between the $\hat{\gamma}$ for two successive values of n_ξ and $m = 1$ is equal to $f^2 \simeq 1/400$ for $F = 10^{-5}$. According to Table 5 of Ref. [5], this ratio ranges from 1/379 to 1/324. A similar statement is made with Eqs. (3) and (4) of Ref. [[4](c)]. Therefore, as in the $n = 2$ case, we believe that our results are qualitatively true.

ROE case. Equations (59)–(61) also apply to ROE states, using the coefficients $c_{\mathbf{M}}$ of (27). At $t^* = 0$, $\bar{\mathbf{v}}_{\mathrm{T}}$ calculated at LO is in the direction of $\bar{\mathbf{L}}\times\mathbf{F}$. This can be checked with the ROE states with $k \equiv 0$, $\beta = -\pi/2$ or $h \equiv N$, $\beta = \pi/2$ in (27). At $t^* > 0$, $\bar{\mathbf{v}}_{\mathrm{T}}(t^*)$ rotates at the Stark frequency about $\hat{\mathbf{z}}$; in Fig. 7 the planar undulating curve should be replaced by a three-dimensional helical curve. For small F/F_{cr} one should observe peaks of $|\bar{\mathbf{v}}_{\mathrm{T}}(t^*)|$ at t^* given by (61). Their number is $n-1$ instead of $n(n-1)$; therefore they should be more discernible than the peaks of $\bar{v}_x(t^*)$ for a CLy state. Another difference with the CLy case is that Stark components of $m \sim n/2$ have an important weight. For these states the approximations (62) and (63) are not valid.

VII. CONCLUSION

We have given theoretical grounds for the existence of a $[\mathbf{v},\mathbf{L},\mathbf{F}]$ asymmetry in strong-field tunneling ionization of an excited hydrogen atom possessing a transverse orbital angular momentum: the extracted electron keeps part of the transverse velocity $\bar{\mathbf{v}}_{\mathrm{T}}$ that it had just before entering the tunnel.

For fields significantly smaller than the mean critical field $\bar{F}^{(0)}_{\mathrm{cr}} \sim 1/(8n^4)$ (in a.u.), the linear Stark effect produces oscillations of $\langle\mathbf{L}_{\mathrm{T}}\rangle$, and therefore of $\langle\mathbf{v}_{\mathrm{T}}\rangle$, making the time-averaged asymmetry very small. A time-resolved experiment is then necessary. For $F \sim \bar{F}^{(0)}_{\mathrm{cr}}$ we predict a sizable time-averaged asymmetry, although our calculations done at lowest order in F greatly overestimate the widths γ_i.

For $n = 2$, the required field is too strong to obtain in a laboratory, at least as a static field. Lasers can produce strong enough, but oscillating, fields. One might nevertheless look for an asymmetry in the lobes and jetlike structure of the photoelectron [41] when the atom initially has an orbital angular momentum perpendicular to the polarization of the laser light.

For $n \gtrsim 10$, the required field has reasonable values, and for $n \gtrsim 20$ a time-resolved experiment can be foreseen. Circular Rydberg states with $\mathbf{L} \perp \mathbf{F}$ and rotating oblique elliptic states are the simplest candidates for a $[\mathbf{v},\mathbf{L},\mathbf{F}]$ experiment. The

latter have the advantage of not being affected by interactions with the electron core. We wrote down analytical formulas generalizing those of the $n = 2$ case. They predict a $[\mathbf{v},\mathbf{L},\mathbf{F}]$ asymmetry in the direction suggested by Fig. 1, at least at leading order in the external field strength.

The preparation of states at a given starting time for a $[\mathbf{v},\mathbf{L},\mathbf{F}]$ experiment is certainly not trivial but, in principle, feasible. Some premature ionization at $t < 0$ is unavoidable but can be limited by approaching the final field from below.

We have restricted our study to ionization in a constant field. One may generalize it to a field $F(t)$ which increases slowly enough so that each Stark component $|\mathbf{M}\rangle$ decays in its turn in the tunneling regime, i.e., while $F(t) < F_{\rm cr}(\mathbf{M})$. The $[\mathbf{v},\mathbf{L},\mathbf{F}]$ asymmetry probably occurs also in the classical ionization regime.

The $[\mathbf{v},\mathbf{L},\mathbf{F}]$ asymmetry, like other angular momentum effects in strong-field ionization [42–44], can lead to a better understanding of the tunnel ionization process itself. It should exist as well in the strong-field *detachment* of electrons from negative ions, with the following advantages: (1) the required field is lower than that for a neutral atom, and (2) there should be no linear Stark effect and hence no oscillation of the asymmetry. An analog of the $[\mathbf{v},\mathbf{L},\mathbf{F}]$ mechanism may also be at work [13,45] in hadron physics, particularly for the Collins effect [46].

ACKNOWLEDGMENTS

We thank J.-M. Richard and M. Shapiro for helping to improve the manuscript and Ch. Bordas for interesting information and suggestions concerning the experimental aspects.

APPENDIX A: DERIVATION OF EQUATION (20)

We first derive Eq. (22) giving $c_{\mathbf{M}}$ for a CLy state $|\bar{\mathbf{A}},\bar{\mathbf{L}}\rangle = |Ly\pm\rangle$ by fitting the asymptotic behaviors of (21) and (19). Let $u \equiv \check{x} + i\,\check{y} = e^{i\phi}\sqrt{\xi/n}$ and $\check{R} \equiv \sqrt{\eta/n}$. For (21) we write $z \pm ix = (\eta - \xi \pm i\sqrt{\eta\xi}\cos\phi)/2 = (n/2)(\check{R} \pm iu)(\check{R} \pm i\bar{u})$, and we obtain

$$\Psi_{Ly\pm}(\mathbf{r}) = [2^N n^2 N!\sqrt{\pi}]^{-1}\, e^{-r/n} \times \sum_{h=0}^{N} C_N^h (\pm iu)^h\, \check{R}^{N-h} \sum_{k=0}^{N} C_N^k\, (\pm i\bar{u})^k\, \check{R}^{N-k}\,. \tag{A1}$$

For (19) we calculate $\Psi_{\mathbf{M}}(\mathbf{r})$ with (5) and the asymptotic form of (7),

$$\Phi_{h,k}(\check{x},\check{y}) \sim (\pi\, h!\, k!)^{-1/2} (\check{x}+i\,\check{y})^h\, (\check{x} - i\,\check{y})^k\, e^{-(\check{x}^2+\check{y}^2)/2}, \tag{A2}$$

obtained by replacing $\partial_{\check{x}}$ by $-\check{x}$ and $\partial_{\check{y}}$ by $-\check{y}$, together with a similar expression for $\Phi_{H,K}(\check{X},\check{Y})$. It gives

$$\Psi_{\mathbf{M}}(\mathbf{r}) \sim n^{-n-1}\, (\pi\, h!\, k!\, H!\, K!)^{-1/2} \times u^h\, \bar{u}^k\, \check{R}^{H+K}\, e^{-(\check{x}^2+\check{y}^2+\check{X}^2+\check{Y}^2)/2}\,. \tag{A3}$$

Recalling $h + K = k + H = N$ and comparing (A1) with (A3), we obtain (22).

We now derive Eq. (20) from (22) using the fact that $\exp(\mathbf{b}\cdot\mathbf{j}_1)$ or $\exp(\mathbf{b}\cdot\mathbf{j}_2)$ transforms a CES into another CES for any real or complex vector $\mathbf{b}$. In particular,

$$|\bar{\mathbf{A}},\bar{\mathbf{L}}\rangle = C\, \exp\{(\lambda_1 - i\beta_1 - i\pi/2)\,\mathbf{j}_1\cdot\hat{\mathbf{z}} + (\lambda_2 - i\beta_2 + i\pi/2)\,\mathbf{j}_2\cdot\hat{\mathbf{z}}\}\,|Ly\pm\rangle\,, \tag{A4}$$

with $e^{\lambda_1} = \bar{h}/(N-\bar{h})$ and $e^{\lambda_2} = \bar{k}/(N-\bar{k})$, gives the most general CES (20) up to a phase. $C = [\cosh(\lambda_1/2)\cosh(\lambda_1/2)]^{-j}$ is a normalization factor.

APPENDIX B: CALCULATION OF THE ASYMPTOTIC TUNNELING WAVE FUNCTION AND OF THE WIDTH

We start from (36) and (37). Neglecting the $(1-m^2)/\eta^2$ term, the roots of $p_\eta^2(\eta)$ (entrance and exit of the tunnel) are $\eta_{\rm in} \simeq -2Z_\eta/\mathcal{E}$, $\eta_{\rm ex} \simeq -2\mathcal{E}/F + 2Z_\eta/\mathcal{E}$. They are slightly complex. We choose the determination

$$p_\eta \simeq (1/2)\sqrt{iF}\,\sqrt{1-\eta_{\rm in}/\eta}\,\sqrt{-i(\eta-\eta_{\rm ex})}\,, \tag{B1}$$

which has cuts along the lines $[0,\eta_{\rm in}]$ and $[\eta_{\rm ex}, -i\infty]$. In the tunnel region $[\mathrm{Re}\,\eta_{\rm in}, \mathrm{Re}\,\eta_{\rm ex}]$ it gives $\mathrm{Im}\,p_\eta(\eta) > 0$, corresponding to an evanescent wave. Beyond the tunnel region it gives $\mathrm{Re}\,p_\eta > 0$, corresponding to an outgoing wave. We assume $\mathrm{Re}\,\eta_{\rm in} \ll \eta_0 \ll \mathrm{Re}\,\eta_{\rm ex} \ll \eta$ and $|S(\eta_{\rm in},\eta_{\rm ex}| \gg 1$. The integration contour in (37) must avoid crossing the cuts of p_η and therefore pass *above* $\eta_{\rm ex}$ in the complex plane. One obtains

$$S(\eta_0,\eta) \simeq \sqrt{-\mathcal{E}/2}\left(\eta_0 + \frac{4\mathcal{E}}{3F}\right) + (\mu/2)\ln\left(\frac{-8\mathcal{E}}{F\eta_0}\right) + (i/3)\sqrt{F}\,(\eta + 2\mathcal{E}/F)^{3/2} + i\pi\mu/2\,. \tag{B2}$$

The first line is $S(\eta_0,\eta_{\rm ex})$; the second is $S(\eta_{\rm ex},\eta)$.

For $\Theta_{\rm St}(\eta_0)$ we use $\eta^{-1/2}\Theta_{\rm St}(\eta) \equiv \Phi_{H,K}(\sqrt{\eta/n},0)$ and Eq. (A2) (changed to capital letters):

$$\Theta(\eta_0) \sim (\pi\, H!\, K!/\nu)^{-1/2}\,(\eta_0/\nu)^{\mu/2}\, e^{-\eta_0/(2\nu)}\,. \tag{B3}$$

Using $p_\eta(\eta_0) \simeq i/(2n)$, $p_\eta(\eta) \simeq \sqrt{F\eta}/2$ in (36), we arrive at the η_0 independent result

$$\Theta_{\rm GS}(\eta) \sim (\pi\, H!\, K!\sqrt{F\eta})^{-1/2}\left(\frac{4}{F\nu^3}\right)^{\mu/2} \exp\left\{\frac{-1}{3F\nu^3}\right\} \times \exp\left\{\frac{i}{3}\sqrt{F}\,(\eta + 2\mathcal{E}/F)^{3/2} + i\pi\mu/2 + i\pi/4\right\}. \tag{B4}$$

The ionization rate is the flux through the paraboloid $\eta = \mathrm{const} \gg n^2$. In the mixed representation (6), it reads

$$\gamma = 2\nu p_\eta\, |\mathcal{N}|^2\, |\Theta(\eta)|^2 \int d\check{x}\, d\check{y}\, |\Phi_{h,k}(\check{x},\check{y})|^2\,. \tag{B5}$$

The last integral equals 1. In $|\Theta(\eta)|^2$ we consider the second line of (B4) to be a pure phase factor, neglecting $\mathrm{Im}\,\mathcal{E}$. One obtains Eq. (39).

[1] L. D. Landau and E. M. Lifshitz, *Quantum Mechanics*, Course of Theoretical Physics Vol. 3 (Pergamon Press, London, 1959).

[2] V. S. Lisitsa, Usp. Fiz. Nauk **153**, 379 (1987) [Sov. Phys. Usp. **30**, 927 (1987)].

[3] T. Yamabe, A. Tachibana, and H. Silverstone, Phys. Rev. A **16**, 877 (1977).

[4] (a) R. Damburg and V. V. Kolosov, J. Phys. B **9**, 3149 (1976); (b) **11**, 1921 (1978); (c) **12**, 2637 (1979).

[5] E. Luc-Koenig and A. Bachelier, J. Phys. B **13**, 1743 (1980).

[6] V. V. Kolosov, J. Phys. B **20**, 2359 (1987).

[7] Yu. N. Demkov, V. D. Kondratovich, and V. N. Ostrovskii, Pis'ma Zh. Eksp. Teor. Fiz. **34**, 425 (1981) [JETP Lett. **34**, 403 (1981)].

[8] V. D. Kondratovich and V. N. Ostrovskii, J. Phys. B **17**, 1981 (1984).

[9] C. Bordas, Phys. Rev. A **58**, 400 (1998).

[10] C. Nicole, H. L. Offerhaus, M. J. J. Vrakking, F. Lépine, and C. Bordas, Phys. Rev. Lett. **88**, 133001 (2002); S. Cohen, M. M. Harb, A. Ollagnier, F. Robicheaux, M. J. J. Vrakking, T. Barillot, F. Lépine, and C. Bordas, *ibid.* **110**, 183001 (2013); A. S. Stodolna, A. Rouzée, F. Lépine, S. Cohen, F. Robicheaux, A. Gijsbertsen, J. H. Jungmann, C. Bordas, and M. J. J. Vrakking, *ibid.* **110**, 213001 (2013).

[11] F. Lépine, S. Zamith, A. de Snaijer, C. Bordas, and M. J. J. Vrakking, Phys. Rev. Lett. **93**, 233003 (2004).

[12] X. Artru and J. Czyzewski, Acta Phys. Pol. B **29**, 2115 (1998).

[13] B. Andersson, G. Gustafson, G. Ingelman, and T. Sjöstrand, Phys. Rep. **97**, 31 (1983).

[14] E. Redouane-Salah and X. Artru, in *The 8th International Conference on Progress in Theoretical Physics (ICPTP 2011)*, AIP Conf. Proc. No. 1444 (AIP, New York, 2012), p. 157.

[15] X. Artru and E. Redouane-Salah, *XV Advanced Research Workshop on High Energy Spin Physics (DSPIN-13)*, edited by A. V. Efremov and S. V. Goloskokov (Joint Institute for Nuclear Research, Dubna, Russia, 2014), p. 41.

[16] T. F. Gallagher, *Rydberg Atoms* (Cambridge University Press, Cambridge, 1994).

[17] H. Friedrich, *Theoretical Atomic Physics* (Springer, Berlin, 1970).

[18] C. Lena, D. Delande, and J. C. Gay, Europhys. Lett. **15**, 697 (1991).

[19] S. Graffi and V. Grecchi, Lett. Math. Phys. **2**, 335 (1978).

[20] C. Cohen-Tannoudji, B. Diu, and F. Laloë, *Mécanique Quantique* (Hermann, Paris, 1977), Vol. 1.

[21] A. K. Kazansky and V. N. Ostrovsky, J. Phys. B **29**, L855 (1996).

[22] P. Bellomo and C. R. Stroud Jr., Phys. Rev. A **59**, 2139 (1999), and references therein.

[23] D. Delande and J. C. Gay, Europhys. Lett. **5**, 303 (1988).

[24] C. Raman, T. C. Weinacht, and P. H. Bucksbaum, Phys. Rev. A **55**, R3995 (1997).

[25] T. P. Hezel, C. E. Burkhardt, M. Ciocca, and J. J. Leventhal, Am. J. Phys. **60**, 324 (1992).

[26] J. C. Gay, D. Delande, and A. Bommier, Phys. Rev. A **39**, 6587 (1989).

[27] R. G. Hulet and D. Kleppner, Phys. Rev. Lett. **51**, 1430 (1983).

[28] W. A. Molander, C. R. Stroud, Jr., and J. A. Yeazell, J. Phys. B **19**, L461 (1986).

[29] J. Hare, M. Gross, and P. Goy, Phys. Rev. Lett. **61**, 1938 (1988).

[30] P. Nussenzveig, F. Bernardot, M. Brune, J. Hare, J. M. Raimond, S. Haroche, and W. Gawlik, Phys. Rev. A **48**, 3991 (1993).

[31] J. C. Day, T. Ehrenreich, S. B. Hansen, E. Horsdal-Pedersen, K. S. Mogensen, and K. Taulbjerg, Phys. Rev. Lett. **72**, 1612 (1994).

[32] D. P. Dewangan, Phys. Rep. **511**, 1 (2012).

[33] M. G. Littman, M. L. Zimmerman, T. W. Ducas, R. R. Freeman, and D. Klepner, Phys. Rev. Lett. **36**, 788 (1976).

[34] J. R. Rubbmark, M. M. Kash, M. G. Littman, and D. Kleppner, Phys. Rev. A **23**, 3107 (1981).

[35] C. H. Cheng, C. Y. Lee, and T. F. Gallagher, Phys. Rev. Lett. **73**, 3078 (1994).

[36] G. Gamow, Z. Phys. **51**, 204 (1928).

[37] A. J. F. Siegert, Phys. Rev. **56**, 750 (1939).

[38] Yu. Slavjanov, *Problemi Matematicheskoi Fiziki* (Lenigrad State University, Leningrad, 1970), pp. 125–134.

[39] M. H. Rice and R. H. Good, Jr., J. Opt. Soc. Am. **52**, 239 (1962).

[40] G. M. Lankhuijzen and L. D. Noordam, Phys. Rev. Lett. **76**, 1784 (1996).

[41] L. Bai, J. Zhang, Z. Xu, and D.-S. Guo, Phys. Rev. Lett. **97**, 193002 (2006).

[42] I. Barth and O. Smirnova, Phys. Rev. A **84**, 063415 (2011); **85**, 029906 (2012); **85**, 039903 (2012).

[43] T. Herath, L. Yan, S. K. Lee, and W. Li, Phys. Rev. Lett. **109**, 043004 (2012).

[44] T. Wang, X. L. Ge, J. Guo, and X. S. Liu, Phys. Rev. A **90**, 033420 (2014).

[45] X. Artru, J. Czyzewski, and H. Yabuki, Z. Phys. C **73**, 527 (1997).

[46] J. Collins, Nucl. Phys. B **396**, 161 (1993).